FACET-BASED TREATMENT ON MICROWAVE BISTATIC SCATTERING OF THREE-DIMENSIONAL SEA SURFACE WITH ELECTRICALLY LARGE SHIP

H. Chen[1], M. Zhang[1, *], and H.-C. Yin[2]

[1]School of Science, Xidian University, Xi'an 710071, China

[2]Science and Technology on Electromagnetic Scattering Laboratory, Beijing 100854, China

Abstract—A feasible simulator, of which formulation and mechanism should be simple and time saving, is developed in this paper to overcome the difficulties of prediction on the EM scattering from three-dimensional (3-D) electrically very large ship-sea models. The work in this paper is twofold. First, the sea surfaces are supposed to be a combination of many locally-tilted slightly rough facets with two-scale profiles. The radar return from each local facet is associated to a semi-deterministic scheme which is established by combining the geometric optics limit of Kirchhoff Approximation (KA-GO) with the Bragg components of Bass-Fuks' two-scale model (BFTSM). Furthermore, we associate the complex reflective function of the respective facet by a so-called Phase-modified Facet Model (PMFM), in which the facet's phase is treated approximately as a combination of inherent part that follows a homogeneous random distribution and coherent part associated with the relative path-delay. Second, in companion with the semi-deterministic treatment of the sea scattering model, a hybrid approximate algorithm is proposed to deal with the composite scattering of electrically large ship-sea model, which is entirely evolved through facets (for the sea surface) and wedges (for the ship target). The method of equivalent currents (MEC) and a hybrid frame which combines the four path model (FPM) with the quasi-image method (QIM) are employed to calculate the scattering characteristics of the ship-like target and ship-sea interactions, respectively. The entire simulator is of comparatively significant computational efficiency, and suitable for providing a preliminary prediction on the instantaneous complex reflective functions and normalized radar cross sections (NRCS) mean levels for electrically very large ship-sea model.

1. INTRODUCTION

Extensive literatures have been devoted to the understanding of electromagnetic (EM) scattering from marine targets especially ships located on the sea surface [1–5]. Several recent publications have centered on fast numerical algorithms based on the well-known method of moments (MoM), which may be listed as the Generalized Forward-Backward (GFB) method [6], multilevel fast multipole algorithm (MLFMA) [7–9], Multiple Sweep Method of Moments (MSMM) [10], etc. Some of these methods have been with mature development and might be able to take charge of the computational burden of the EM scattering from three-dimensional (3-D) electrically very large targets. Nevertheless, they are still unsuitable for virtual usage due to the intractable computational complexity caused by the random variation of the large scope sea surface. Consequently, in terms of feasibility and practicability, another tractable means based on the high frequency asymptotic method seems more flexible and suitable for the issue, such as Geometrical Optics (GO), Physical Optics (PO), Geometrical Theory of Diffraction (GTD), Physical Theory of Diffraction (PTD). Apparently, the asymptotic methods are much faster than the pure numerical methods while facing the electrically large model. One important bottleneck of the asymptotic method is the modeling accuracy of the multipath EM interaction between the ship and sea. The techniques as Shooting and Bouncing Rays (SBR) [11, 12], Iterative Physical Optics (IPO) [2, 13], etc. have also been introduced to obtain a more accurate evaluation on the ship-sea interactions. However, more or less, the aforementioned models were established for two-dimensional (2-D) models, focused on the horizontal polarization with application to conditions of Perfect Electric Conductors (PEC), only accounted for special kinds of simplified obstacles, or alternatively given simulations on monostatic or bistatic scattering. Besides, methods even as SBR and IPO also face the problem of too severe computational load to give a fast solution to the composite scattering problem when the comprehensive ship-sea model being treated as a whole in electrically very large size. Complexities due to the large size and intricate multi-interactions make the model simulation much more awkward, and as a result, the intensive study of fast and feasible scattering model for the issue is still of great sense. In our opinion, approximate strategies, as dihedral/three-plate corner simplification [4, 14, 15], four-path model combined with high frequency asymptotic methods [16, 17], or hybrid scheme with MEC and IPO [2] are attractive and feasible at this stage.

    It is generally accepted that the sea surface has much influence on

the radar reflectivity of the ships. In most of the relevant publications available, while modeling the whole ship-sea model, the sea surface might be always treated as one dimension, PEC condition, or a combination of many flat facets where only the coherent scattering is accounted for. However, it was reported that the Bragg scattering process governs the mechanism of backscattering from sea surface for moderate wind speeds and incident angles away from nadir and grazing [18–21]. Attempts have been made over years to build a unified theory that can overwhelm most of the issues associated with the radar scatter estimation on sea surface. The kernel of two scale theory [19, 22, 23], one of the famous approaches, is the artificial division of the real surface with two types of irregularities. One of the earlier two-scale formulas is accomplished by Fung and Lee [23]. They evaluated the large scale tilt effect by averaging the backscattering cross section from perturbation theory over the large scale slopes' probability distribution. Their model has a statistical scheme, which encompasses both large waves and small ripples to obtain an average of the real diffusion coefficient without a particular sea height map. Although they give an average line budget, nothing is said about the instantaneous complex reflection corresponding to the local spatiality characteristics on the deterministic profile of a special sea surface. Therefore, the deterministic application of the two-scale theory [26, 27], which tries to break radar cross sections (RCS) returns into the instantaneous one, is more attractive for the application to ship-sea composite scattering, as well as ocean synthetic aperture radar (SAR) imagery simulations [4, 24, 25].

The main motivation of this paper is establishing a feasible tool for the RCS calculation of a ship-sea model, which can offer preliminary evaluation on sea returns. The formulation and mechanism should be simple and time saving so as to overwhelm the bottle neck of the application to 3-D electrically large models. In the previous work [28], a so called "Slope/Semi-Deterministic Facet Model (SDFM)" has been involved, in which the elementary radar returns from respective facets are computed by a semi-deterministic scheme combining KA-GO with Bragg components of the original BFTSM, as well as extension to bistatic case. As intensively concerned, it is significant to evaluate the complex reflectivity function to enable one's model to be a useful implement not only for modeling the composite scattering but also for developing an ocean SAR simulator. Due to implementation of this application, we do consider the extension for the phase distribution of the facet returns a useful and urgently needed work. In most of the relevant papers [26, 29], the fields received from different facets were generally assumed to be with independent random phases drawn

from uniform random numbers between 0 and 2π. This assumption indicates that the phases are well decorrelated so that the total cross section can be obtained by averaging cross sections from all facets. In this paper, a preliminary consideration for the extension is made, which simply associates the facet phase with the relative path-delay of the individual scatterers. Along with all the aforementioned extensions, we develop a so-called "Phase-modified Facet Model (PMFM)", which is easy to implement and performs well in the evaluations on the mean levels of both the monostatic and bistatic NRCS.

Furthermore, on the basis of the PMFM, a hybrid approximate algorithm of comparatively significant computational efficiency is proposed to deal with the composite scattering of electrically large ship-sea scattering model. The method of equivalent currents (MEC) [30, 31] and the hybrid scheme which combines the four path model (FPM) with the quasi-image method (QIM) [16, 17, 32, 33] are devoted to analysis of the EM scattering emerging from the ship and the EM interaction between the ship and sea surface, respectively. This kind of hybrid scheme allows us to obtain a fast prediction on the mono- and bistatic RCS mean levels from a generally 3-D maritime scene with electrically large ship-like target. Several numerical examples are given in Section 4 to confirm the validity and practicability of the proposed simulator.

2. MODEL DESCRIPTION OF FACET SCATTERING

A major simplification of the facet scattering theory follows from the hypothesis that the returns at different points on the sea surface are uncorrelated. This assumption has been confirmed by the experimental results of the earlier explicit backscattering models [18, 34], which demonstrate that sea backscatter decorrelates spatially quite rapidly at microwave frequencies. We make this hypothesis throughout the model development as well. As preparation, the surface is envisaged as a frozen instantaneous sea surface state and locally approximated by plane facets, centered on the grid points that geometrically described by a discrete set of $z = h(\mathbf{r})$ and the corresponding slopes $z_x = \partial h/\partial x$, $z_y = \partial h/\partial y$. The large scale structure of the sea surface is generated by the linear statistical spectra model on the basis of the JONSWAP spectrum [35]. More detailed description could be found in [36].

In the following context, the study on facet approach begins with the bistatic and non-Gaussian spectrum extension of the original formula of Bass and Fuks' composite model. The geometry of the scattering surface is discussed and shown in Figure 1. We consider a plane wave $\mathbf{E}_{inc} = \hat{\mathbf{p}}_0 E_i \exp(ikR)$ incidents on a statistically dielectric

surface, which is assumed to be a combination of myriads of large-scale facets with small ripples $z_s = h_s(\mathbf{r})$ ride on. $\hat{\mathbf{p}}_0$ is the unit polarization vector of the incident wave, and R is the distance from the sensor to the point on sea surface. The vertical deviation of $z_s = h_s(\mathbf{r})$ from the mean plane of large-scale facet is described by a random function with $\bar{h}_s = 0$, $\overline{h_s^2} = \sigma_s^2$, $\langle h_s(\mathbf{r}) h_s(\mathbf{r} + \Delta\mathbf{r}) \rangle = \sigma_s^2 \rho_s(\mathbf{r})$, where ρ_s is the spatial autocorrelation function and σ_s^2 the height variance of the small ripple at resonant scattering wave number.

According to the two scale scattering model presented by Bass and Fuks [22], the scattering field emerging from a dielectric rough surface is expressed by

$$\mathbf{E}_s = \frac{k^2 \exp(ikR)}{\pi R} E_i \int_S \mathbb{S}_{TSM} h_s(\mathbf{r}) \delta(\mathbf{r}, \hat{\mathbf{K}}_0, \hat{\mathbf{K}}) \exp(-i\mathbf{Q} \cdot \mathbf{r}) d\mathbf{r} \quad (1)$$

where $\mathbf{Q} = k(\hat{\mathbf{K}}_0 - \hat{\mathbf{K}})$; $k = 2\pi/\lambda$ is the electromagnetic wave number of wave, λ the incident wave length, $\hat{\mathbf{K}}_0$ the vector directed from the transmitter. $\hat{\mathbf{K}}$ is the one directed to the reception point and with the unit polarization vector $\hat{\mathbf{p}}$; $\delta(\mathbf{r}, \hat{\mathbf{K}}_0, \hat{\mathbf{K}})$ is for the possible shadowing of the sea surface and may have two values 1 and 0 depending on whether the facet is illuminated or not. The polarization-dependent functions $\mathbb{S}_{TSM}$, in general, depend on the incident and scattering angles, polarizations, as well as the local normal unit of each facet. Their detailed expressions are derived in [28].

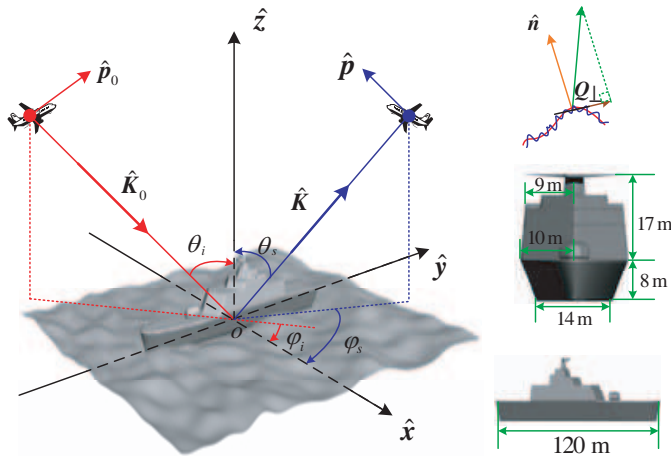Since the scattering field in the bistatic formula of BFTSM is

Figure 1. Coordinate axes and geometry of ship and sea surface.

obtained by Equation (1), in the case of a unit incident wave, the general form of a facet's scattering coefficient can be expressed by.

$$\sigma_{TSM}^{facet}(\hat{\mathbf{K}}_0, \hat{\mathbf{K}}) = 8k^4\delta(\mathbf{r}, \hat{\mathbf{K}}_0, \hat{\mathbf{K}})\, \mathbb{S}_{TSM}\mathbb{S}_{TSM}^* W(\mathbf{Q}_\perp) \qquad (2)$$

$\mathbf{Q}_\perp = \mathbf{Q} - \hat{\mathbf{n}}(\hat{\mathbf{n}} \cdot \mathbf{Q})$ is the projection vector of $\mathbf{Q}$ to the plane facet, and with coordinates of $(Q_\perp, \phi_\perp)$. $\hat{n}$ points in the normal direction of the large-scale facet. $W(\mathbf{Q}_\perp) = 2\pi\sigma_s^2 G_s(Q_\perp) f(Q_\perp, \phi_\perp - \phi_w) = 2\pi W_p(Q_\perp) f(Q_\perp, \phi_\perp - \phi_w)/Q_\perp$, wherein $W_p(\cdot)$ is the Pierson's capillary spectrum given by Fung and Lee [23], $G_s(\cdot)$ the Fourier transform of the ripple correlation function $\rho_s(\mathbf{r})$, and $f(\cdot)$ the spreading function. The shadowing factor δ is realized with the help of a frequently used algorithm for computer graphics: the Z-Buffer technology [37]. Therefore, from Equation (2), it could be concluded that the returns from different facets are proportional to the instantaneous Bragg components of the capillary spectrum, which leads to semi-statistical independence.

As a numerical method, the large-scale sea surface can be represented approximately by sufficiently small plane facets, centered on the grid points. Accordingly, some facets may be in a diffuse configuration, while others in a specular configuration. It has clear physical grounds to revise the TSM by a combination of KA with TSM contributions, rather than adding KA to SPM, so called semi-deterministic approach [27]. In order to apply the two-scale Bragg theory, the facet must be large in comparison with the wavelength of the incident radiation, and be sufficiently small as it can still be regarded as a plane. We postulate that the discrete facets are in proper size, so that the KA and TSM can be used in the local summation frame. Then, the return from each facet can be expressed by

$$\sigma^{pop}\left(\hat{\mathbf{K}}_0, \hat{\mathbf{K}}\right) = \frac{1}{A}\delta\left(\mathbf{r}, \hat{\mathbf{K}}_0, \hat{\mathbf{K}}\right) \sum_{i=1}^{M}\sum_{j=1}^{N}\left[\Delta x \Delta y\left(\sigma_{ij,KA}^{P_0 P} + \sigma_{ij,TSM}^{P_0 P}\right)\right]\Bigg|_{x_{ij} > \cot\theta_i} \qquad (3)$$

$$\sigma_{ij,KA}^{p_0 p}\left(\hat{\mathbf{K}}_0, \hat{\mathbf{K}}\right) = \frac{Q^2\pi k^2}{Q_z^4}\left|\mathbb{S}_{KA}\right|^2 \mathbf{Prob}\left(-Q_x/Q_z, -Q_y/Q_z\right) \qquad (4)$$

$$\sigma_{ij,TSM}^{p_0 p}\left(\hat{\mathbf{K}}_0, \hat{\mathbf{K}}\right) = 8k^4\, \mathbb{S}_{TSM}\mathbb{S}_{TSM}^* W(\mathbf{Q}_\perp) \qquad (5)$$

$\mathbb{S}_{KA}$ is polarization-dependent coefficients [39],

$$\mathbb{S}_{KA}^{hh} = \gamma[\rho_{0_v}(\hat{\mathbf{p}}_h \cdot \hat{\mathbf{K}}_0)(\hat{\mathbf{p}}_{0h} \cdot \hat{\mathbf{K}}) + \rho_{0_h}(\hat{\mathbf{p}}_v \cdot \hat{\mathbf{K}}_0)(\hat{\mathbf{p}}_{0v} \cdot \hat{\mathbf{K}})] \qquad (6)$$

$$\mathbb{S}_{KA}^{vv} = \gamma[\rho_{0_v}(\hat{\mathbf{p}}_v \cdot \hat{\mathbf{K}}_0)(\hat{\mathbf{p}}_{0v} \cdot \hat{\mathbf{K}}) + \rho_{0_h}(\hat{\mathbf{p}}_h \cdot \hat{\mathbf{K}}_0)(\hat{\mathbf{p}}_{0h} \cdot \hat{\mathbf{K}})] \qquad (7)$$

$$\mathbb{S}_{KA}^{hv} = \gamma[\rho_{0_v}(\hat{\mathbf{p}}_h \cdot \hat{\mathbf{K}}_0)(\hat{\mathbf{p}}_{0v} \cdot \hat{\mathbf{K}}) - \rho_{0_h}(\hat{\mathbf{p}}_v \cdot \hat{\mathbf{K}}_0)(\hat{\mathbf{p}}_{0h} \cdot \hat{\mathbf{K}})] \qquad (8)$$

$$\mathbb{S}_{KA}^{vh} = \gamma[\rho_{0_v}(\hat{\mathbf{p}}_v \cdot \hat{\mathbf{K}}_0)(\hat{\mathbf{p}}_{0h} \cdot \hat{\mathbf{K}}) - \rho_{0_h}(\hat{\mathbf{p}}_h \cdot \hat{\mathbf{K}}_0)(\hat{\mathbf{p}}_{0v} \cdot \hat{\mathbf{K}})] \qquad (9)$$

where $\gamma = Q \Big/ \Big\{ [(\hat{\mathbf{p}}_h \cdot \hat{\mathbf{K}}_0)^2 + (\hat{\mathbf{p}}_v \cdot \hat{\mathbf{K}}_0)^2] k \Big\}$. The large scale surface is facetized by the number of M and N along x and y axes, respectively; Δx and Δy indicate the facet range along x and y direction; A is the area of the sea surface; ρ_{0_v} and ρ_{0_h} are the Fresnel reflection coefficient for vertical and horizontal polarization respectively. The definitions of $\hat{\mathbf{p}}_{0h}$, $\hat{\mathbf{p}}_{0v}$, $\hat{\mathbf{p}}_h$ and $\hat{\mathbf{p}}_v$ can been found in [28], and **Prob** $(\cdot)$ is the Cox-Munk PDF [38]. The slopes over z_x have to be limited by $-\cot\theta_i$ to account for the shadowing by large scale waves. In order to filter out the roughness components (some facets) for which the small perturbation method is inadequate, we limit the contribution of $W_p(Q_\perp)$ by an artificial cut-off wave number. It remains no unified guideline for the selection of the cutoff wave number. Different authors make different choices. Here, we choose $k/3$ empirically. Equation (3) is basically used to evaluate the individual scattering coefficients from facet elements and involved as the so called "extended BFTSM (EBFTSM)".

By now, we use a so called "facet-based approach" to the sea scattering model, which tries to break the surface into local plane facets. The Bragg contribution of each facet is determined by the BFTSM, and the KA-GO is employed to help the EBFTSM to take charge the specular zone correctly. We call this procedure a "semi-deterministic" approach. With the help of this effort, the return map of a deterministic sea profile can be readily obtained. We found that the EBFTSM can reflect the local scattering characterizations (on the view of the amplitude of the scattering function) of two-scale profiles: as shown in Figure 2, the sea state is at a wind speed of 5 m/s; the relative dielectric constant of the sea water is calculated by the Klein dielectric constant model [40] at $20°$ and $35‰$ salinity; the incident wave is at 14 GHz and VV polarization; (a) and (c) are with the sea elevations in the wind direction of $0°$ and $60°$, respectively; (b) and (d) display the corresponding return maps in the backscattering observations along the wind directions.

3. PHASE-MODIFIED FACET MODEL (PMFM)

It is not sufficient to make one's model overcome the difficulties in the application to ship-sea composite scattering only with the evaluation on the mean levels (amplitude) of instantaneous return from each facet. To implement the application, we do consider the predictions for not only the amplitude but also the phase distribution of the facet's return a useful and urgently needed work. Since the averaged RCS has been locally changed for facets. In other words, the individual amplitude of the fields received from the facet could be readily obtained by using
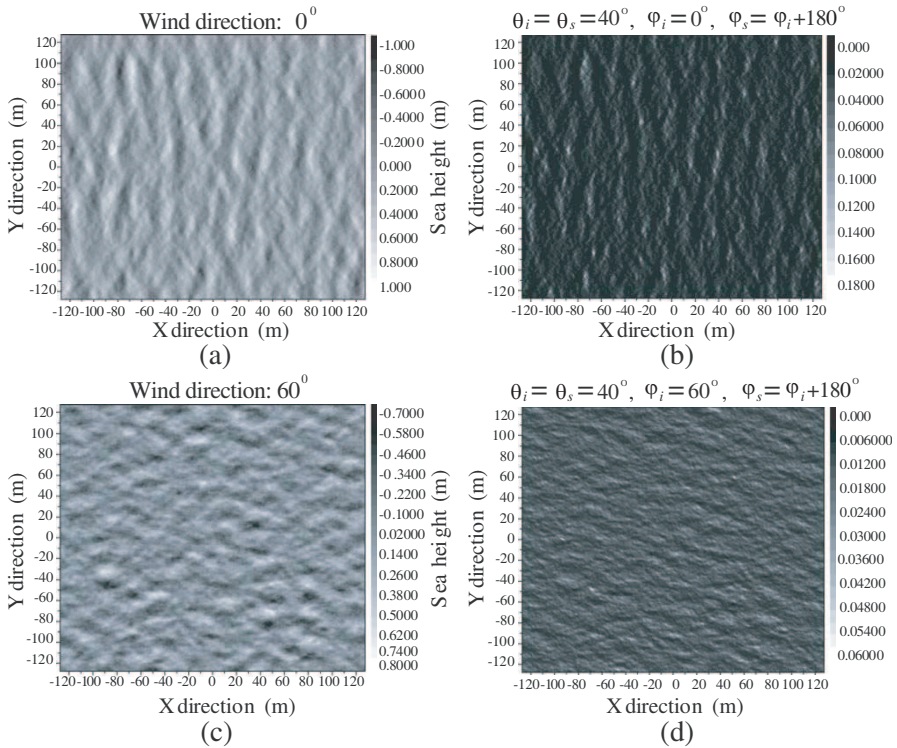
Figure 2. Return map of a deterministic sea profile: (a) and (c) are with the sea elevations in the wind direction of $0°$ and $60°$, respectively. (b) and (d) display the corresponding return maps in the backscattering observations along the wind directions.

the EBFTSM. The key issue is the modeling of the phase characteristic of each facet. In general, the total scattering field E_s received from N_s scatterers on the digital sea map is the resultant of the phasors of individual scatterers [43]:

$$\mathbf{E}^S = \sum_{k=1}^{N_s} E_k^S \exp(i\varphi_k) \exp\left(i\frac{2\omega R_k}{c}\right) \qquad (10)$$

Here, E_k^S and φ_k are, respectively, the amplitude and inherent phase associated with the kth scatterer. The phase term $\exp(i2\omega R_k/c)$ is associated with the path-delay of the echo from the kth scatterer. The following notations are in order. ω is the angular frequency, c the speed of light, R_k the range of the kth scatterer, and N_s the number of scatterers. Under the aforementioned hypothesis, the decorrelation

of phases is essentially implied. Moreover, within the isolated facet scatterer, the phases may be regarded as spatially white. Being inspired by the isotropic assumption, we decide to treat each inherent phase φ_k as a variable that follows a homogeneous random distribution denoted by $\Delta\varphi_{\max}\zeta$. $\Delta\varphi_{\max}$ is the maximum phase difference from the front edge and the back edge of a facet, and ζ is a random number between -0.5 and 0.5. Accordingly, only the path delay term given by $2\omega R_k/c$ contributes to the directionality of the scattering pattern. Then, the total return E^{sea} can be written in the following summation form:

$$E^{sea}=\sum_{i=1}^{M}\sum_{j=1}^{N}\left[\frac{\exp(ikp)\delta(\cdot)}{R}\sqrt{\frac{\Delta x\Delta y}{4\pi}\left(\sigma_{ij,KA}^{P_0 P}+\sigma_{ij,TSM}^{P_0 P}\right)}\exp\left(-i\varphi_{ij}^{add}\right)\right]\Bigg|_{z_{x,ij}>-\cot\theta_i\phi} \tag{11}$$

The additional phase φ_{ij}^{add} of each facet can be expressed by

$$\varphi_{ij}^{add} = \Delta\varphi_{\max}\zeta + \Delta\rho_{ij} \tag{12}$$

wherein $\Delta\varphi_{\max} = Q_x\Delta x + Q_y\Delta y + Q_z\left(z_x\Delta x + z_y\Delta y\right)$ is the maximum phase difference and $\Delta\rho_{ij} = \mathbf{Q}\cdot\mathbf{r}$ the delay path of each scatterer.

Equation (11) represents the total field that evaluated over one frozen surface. The averaged scattering coefficient coming from M_s samples can be given by

$$\bar{\sigma} = \frac{1}{M_S}\sum_{m=1}^{M_S}\left[4\pi\lim_{R\to\infty}\left(R^2\mathbf{E}_m^{sea}\mathbf{E}_m^{sea^*}/A\right)\right] \tag{13}$$

Up to now, we simply counted the relative coherent phase delay of each facet. This approximation might be only sufficient for a stationary large scale profile, rather than a time evolving surface. As a fact, this "approximate phase distribution" is not exact enough to account for the microstructure (Bragg ripples) imposed on each plane facet. Thus, it might not be able to build a real phase distribution that determines the Doppler spectra as a function of time delay. To get a more exact simulation of the phase distribution, one could improve the phase factor with a short wave modification of the facet, which is similarly accomplished by [44]. Nevertheless, since the main discussion of the paper is based on a stationary scene, the Doppler effect is not concerned temporarily and beyond this paper. Although the "approximate phase distribution" still needs further validation on physical explanation and in-depth analysis, from Figure 3, we find that the averaged coefficient with the phase approximation mainly remains in accordance with the former line evaluated by EBFTSM for both co- and cross-polarizations, which indicates that the scattering field governed by Equation (11) might be with validity on the view of

mean levels at least. In addition, in the simulations, the sea surface is generated at $5\,\mathrm{m/s}$, upwind direction. The area is $256 \times 256\,\mathrm{m}^2$, with the grid of $1 \times 1\,\mathrm{m}^2$. The proper selection of the facet dimension is required to ensure the decorrelation of the phasor returns from different facets. Plant [45] found that the decorrelation lengths for sea return at both X- and Ka-band were about 10 times the microwave length. Therefore, the decorrelation length (facet dimension) needs to be at
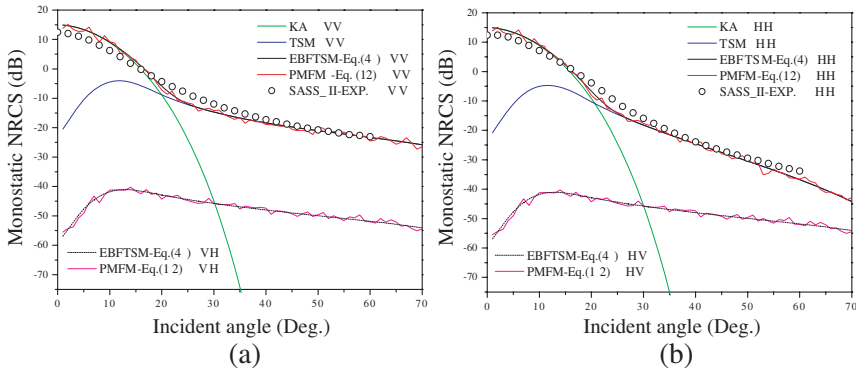

Figure 3. Agreement tests in monostatic case between the EBFTSM, PMFM and the averaged Ku band experiment data drawn from SASS-II [41]. The scattering coefficients are averaged over 30 samples in application of PMFM. (a) For VV and VH polarizations. (b) For HH and HV polarizations.
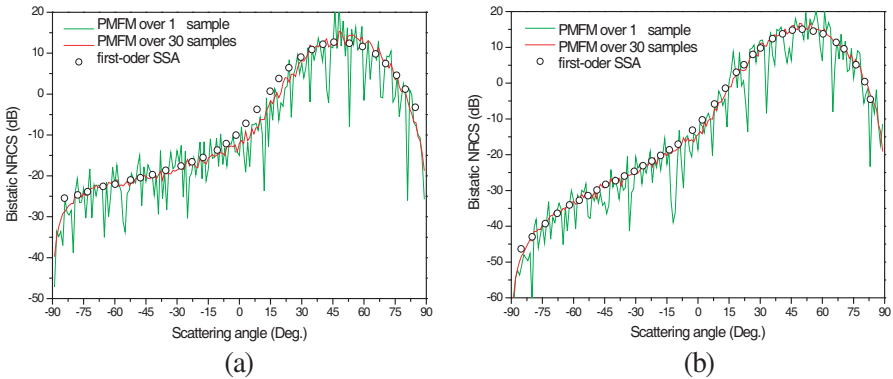

Figure 4. Agreement tests on the bistatic configuration of for-back scattering bewteen the PMFM and first-order SSA. The parameters are fixed as: $\theta = 50°$, $\varphi_i = \varphi_s = 0°$. (a) For VV polarization. (b) For HH polarization.

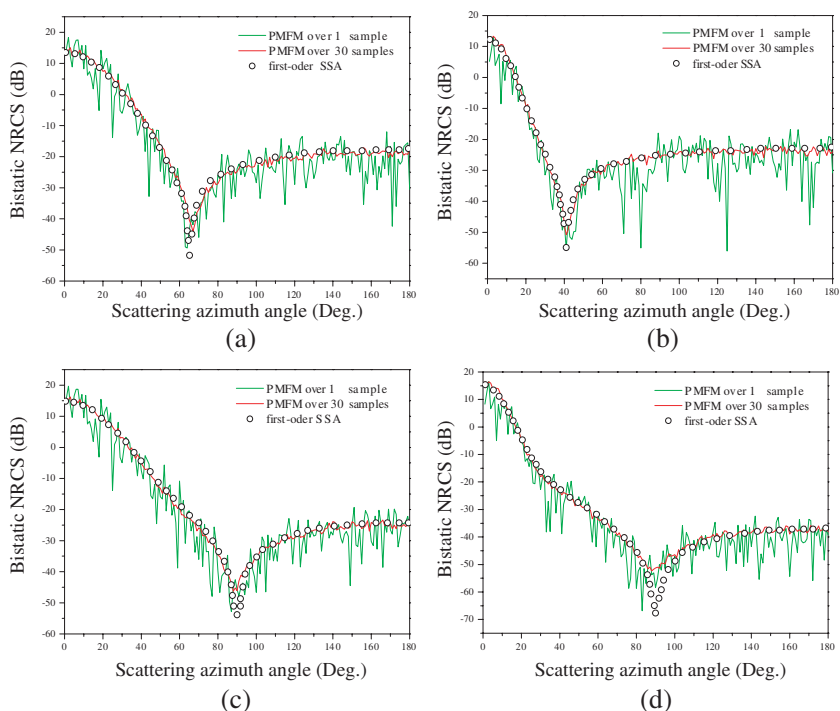**Figure 5.** Comparison on the bistatic NRCS versus φ_s between the results yielded by the first order SSA and that by PMFM. The parameters are fixed in order. (a) $\theta_i = \theta_s = 40°$, $\varphi_i = 0°$, VV polarization. (b) $\theta_i = \theta_s = 60°$, $\varphi_i = 0°$, VV polarization. (c) $\theta_i = \theta_s = 40°$, $\varphi_i = 0°$, HH polarization. (d) $\theta_i = \theta_s = 60°$, $\varphi_i = 0°$, HH polarization.

least about 0.21 m in Ku band so that the fields emerging from different facets are well decorrelated. However, the facet should also be small enough so as to sufficiently reflect the geometry characteristics of the large scale sea surface. Experimentally, the average NRCS does not much depend upon the facet size changed from 0.5 m to 1.5 m.

Examples of the bistatic NRCS functions evaluated over 1 sample and that averaged over 30 samples are shown in Figure 4 and Figure 5. The parameters of the sea surface generation are the same as Figure 3. The incident wave frequency is fixed as 14 GHz. The validations on the bistatic configurations are mainly performed with comparisons between the model and the first-order small slope approximation (SSA) [42]. Figure 4 shows comparisons on the bistatic configuration of for-back scattering defined by $\theta_i = 50°$, $\varphi_i = \varphi_s = 0°$, (a) for VV polarization

and (b) for HH polarization. Apparently, the variability in average is much less than the non-averaged one, and the maximum energy is received around the specular direction $50°$, which is a logical result. The results of another test are shown in panels (a)–(d) of Figure 5 to check the bistatic performances along with the variations of the scattering azimuth angle φ_s from $0°$ to $180°$. The NRCS lines reach their low peaks when the receiving polarization vector locates in the orthogonal plane of incident polarization vector. Thus, as observed, for HH polarizations, the position of the peak always occurs at $\varphi_s = 90°$; for VV polarizations, their peaks depend on the incident angle and locate at lower φ_s with the θ_i increasing from $40°$ to $60°$. In conclusion, the behaviors of all the aforementioned curves appear reasonable with similar trends and excellent agreements with that disclosed in other relevant papers [27, 42], which indicates that the model results perform quite well and could give reliable prediction on the mean levels of both mono- and bistatic NRCS values.

4. COMPOSITE SCATTERING OF A SHIP AT SEA

Great efforts have been devoted to tackling the interaction between the ship-like target and sea surface. Due to the computational burden and memory requirements, most of the numerical algorithms and asymptotic methods, even as IPO and SBR, are virtually not applicable to ship-sea model in electrically large size. Accordingly, the approximate techniques would be attractive as they have a more applicable formulation that should be simple and time saving. The four path model was firstly released by Johnson [32], and was simply involved by Shtager [33] in the estimation of sea surface influence on radar reflectivity of ships, which has been generally regarded as an efficient scheme for the computation of the multiple scattering between the ship and sea surface. Relative works on the application of this model to marine scene have been reported in [16, 17].

The scattering mechanism of the four path model is illustrated in Figure 6(a). According to this model, only a single scattering interaction between the ship and flat sea surface is under consideration. The interactive paths are involved equivalently as a so-called "bistatic scattering" from the ship target on the basis of the quasi-image method (QIM). In other words, they are calculated as if the target was in free space, and one or two appropriate reflection coefficients are included in the scattered field amplitude. The four paths are equivalently denoted as follows, Path-1: I → II, Path-2: I → II → IV, Path-3: IV → II → III, and Path-4: V → II → III → VI.

By using the MEC [30, 31], the scattering fields from the ship-like
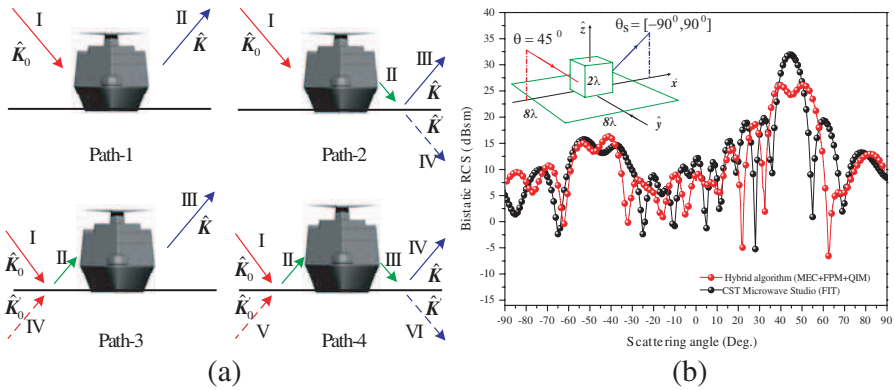
Figure 6. Description and validation on the composite scattering of a target at sea: (a) Multi-path model of the quasi-image method; (b) Agreement test between the hybrid algorithm and finite integral technique.

target (Path-1) is:

$$\mathbf{E}_S^{ship} = \sum_{i=1}^{N} \mathbf{E}_i^{wedge}\left(\hat{\mathbf{K}}_0, \hat{\mathbf{K}}\right) \tag{14}$$

N is the number of the wedges, and E_i^{wedge} is the scattering field from the wedge i and given by

$$\mathbf{E}^{wedge} = \frac{-ik}{4\pi R} \int_C \left[\eta_0 I(\mathbf{r}')\hat{\mathbf{K}} \times \left(\hat{\mathbf{K}} \times \hat{\mathbf{t}}\right) + M(\mathbf{r}')\left(\hat{\mathbf{K}} \times \hat{\mathbf{t}}\right)\right] \exp(ik\hat{\mathbf{K}} \cdot \mathbf{r}')dl \tag{15}$$

where η_0 is the intrinsic impedance of the medium, $\mathbf{r}'$ the position of a point on the edge C of each wedge, $\hat{\mathbf{t}}$ the unit vector along the edge, and I and M the equivalent edge currents assumed at the edge of a planar scattering.

The total scattering field E^{wedge} is calculated by a sum of two components: the Physical Optics (PO) scattering and the diffraction scattering field, i.e.,

$$\mathbf{E}^{wedge} = \mathbf{E}_{PO}^{wedge} + \mathbf{E}_{PTD}^{wedge} \tag{16}$$

Here we use PO for calculation of coherent scattering from faces and PTD for the calculation of diffraction from edges. $\mathbf{E}_{PO}^{wedge}$ and $\mathbf{E}_{PTD}^{wedge}$ are calculated with the improved edge currents I^{PO}/M^{PO} and I^{PTD}/M^{PTD} by modified edge representation, which are obtained with the help of PO theory and physical theory of diffraction (PTD). The detailed expressions of I^{PO}/M^{PO} and I^{PTD}/M^{PTD} can be found in

our published paper [31]. Then, the scattering fields from the ship-like target can be calculated with the help of Equations (14)–(16).

It has been generally suggested that the comprehensive ship-sea model can be treated as PEC for HH polarization at high incident frequencies [13]. Actually, the complex reflection coefficient of sea surface should be treated as follows [14]:

$$\rho = \rho_0 \rho_s \tag{17}$$

ρ_0 is the Fresnel reflection coefficient and ρ_s the specular reflection factor defined as

$$\rho_s = \begin{cases} \exp\left[-2\left(2\pi\tau\right)^2\right] & 0 \le \tau \le 0.1 \\ 0.812537 \Big/ \left[1 + 2\left(2\pi\tau\right)^2\right] & \tau > 0.1 \end{cases} \tag{18}$$

where $\tau = \sigma_h \cos\theta_i / \lambda$, λ is the incident wave length, and σ_h the root mean square (RMS) of the sea roughness (m).

With the help of the complex reflection coefficient ρ, we could readily represent the coupling scattering field by the following equations under the four path diagram (Path-2, Path-3 and Path-4):

$$\mathbf{E}_S^{cou} = \sum_{i=1}^{N} \rho \mathbf{E}_i^{wedge}\left(\hat{\mathbf{K}}_0,\ \hat{\mathbf{K}}'\right) + \sum_{i=1}^{N} \rho \mathbf{E}_i^{wedge}\left(\hat{\mathbf{K}}_0',\ \hat{\mathbf{K}}\right)$$
$$+ \sum_{i=1}^{N} \rho^2 \mathbf{E}_i^{wedge}\left(\hat{\mathbf{K}}_0',\ \hat{\mathbf{K}}'\right) \tag{19}$$

Figure 6(b) gives a comparison between the result evaluated by the proposed hybrid algorithm and the one simulated with the help of CST Microwave Studio, which involves the so called finite integral technique (FIT) to calculate the EM field emerging from 3-D targets. The validation example of a 2λ cube over an 8λ square plane is calculated at $1.0\,\text{GHz}$ for HH polarization. And for the sake of brevity, all the examples discussed in this content are fixed at HH polarization. The incident angle is $45°$, and the scattering angle varies from $-90°$ to $90°$. The incident and scattering azimuth angle are fixed at $0°$. It can be seen that the hybrid result is in comparative accordance with the line by CST. Disagreements may occur at the specular direction around $45°$ and near grazing observation angles, which may be caused by the inherent deviation of the simplification of FPM. However, the FPM can save much more time than the FIT (for ordinary personal computer with $2.5\,\text{GHz}$ CPU ($2.0\,\text{GB}$), the consumed time is $364.8\,\text{s}$ for FPM but more than 10 hours for FIT), while sufficient accuracy could mainly be in assurance. This advance makes the FPM a very attractive and

promising scheme to take charge of the intractable work on modeling of EM scattering from electrically large ship at sea.

Recalling to Section 3, we could readily obtain the sea return E^{sea} by using Equation (11). Therefore, the total scattering field from the ship-sea model is treated as a superimposition of the scattering contributions from sea, ship target and interactions:

$$\mathbf{E}_S^{total} = \mathbf{E}^{sea} + \mathbf{E}_S^{ship} + \mathbf{E}_S^{cou} \tag{20}$$

Then, the radar cross section of the comprehensive ship-sea model is calculated by:

$$RCS = 4\pi \lim_{R \to \infty} R^2 \left| \mathbf{E}_S^{total} \right|^2 \Big/ \left| \mathbf{E}_{inc} \right|^2 \tag{21}$$

In the following discussion, the 3-D sea surface is simulated at wind speed of $1\,\mathrm{m/s}$, crosswind. The grid is set to $1 \times 1\,\mathrm{m}^2$, with the sea area $500 \times 200\,\mathrm{m}^2$. The ship-like target is subdivided into triangular facets with the help of CAD tools. Its geometrical parameters are shown in Figure 1. On the basis of the hybrid algorithm, the bistatic examples are discussed in Figure 7. The simulation is computed for incident on the broadside ($\theta_i = 40°$, $\phi_i = 90°$) and at HH polarization. It can be seen that the presence of a ship significantly enhances the bistatic scattering in the whole backward direction. In the forward direction, scattering is dominated by the sea surface contribution, especially at the specular direction. The peak value at c point is caused by the contribution of direct scattering from the complex geometry of ship body, see Figure 7(a). Figure 7(b) shows the multipath interactions between ship and sea surface. The peaks at b and e are resulted from the interaction with Path-2, while a and d are associated with Path-3. The contribution of Path-4 is ignored because it has much lower value than the other two paths. In addition, it is worthwhile to point out that such a kind of simulation is much tractable and time-saving for personal computers to take charge of.

Several examples of the monostatic RCS of a ship at sea is shown in Figures 8(a)–(d). The parameters are fixed as follows: the elevation angle is varied from $0°$ to $180°$; the azimuth angle is set to $0°$ for (a), (c) and $90°$ for (b), (d); the incident wave frequency is $8.0\,\mathrm{GHz}$ for HH polarization; and the wind speed is set as $4\,\mathrm{m/s}$ for (a), (b) and $7\,\mathrm{m/s}$ for (c), (d); the wind direction is in upwind case. From these figures, it can be seen that, when incident from the endwise ($\varphi_i = 90°$), the surface significantly enhances the RCS in particular directions such as $10°$, $30°$, $45°$, $165°$, and $175°$, while incident from the broadside ($\varphi_i = 0°$), and the peaks occur at $5°$, $47.5°$, $132.5°$, and $175°$. Besides, as the sea surface becomes rough with the wind speed increasing, its
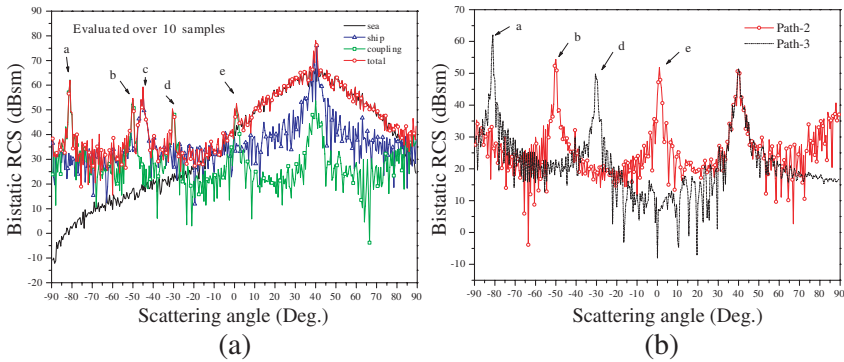
Figure 7. Composite scattering of a ship-sea model at 3 GHz, HH polarization. (a) Bistatic RCS of the ship-sea model. (b) Multipath interactions between ship and sea surface.
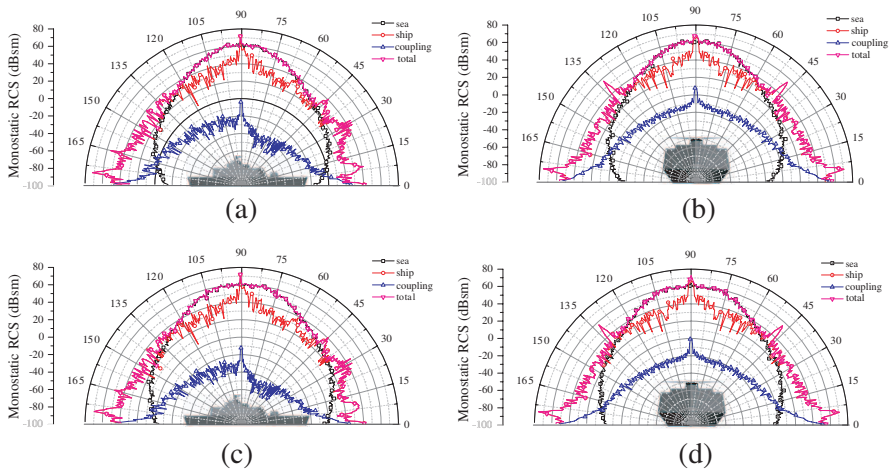

Figure 8. Monostatic RCS of the ship-sea model.

influence on the RCS is less in the specular directions and much in the near grazing directions.

5. CONCLUSION

The simulator proposed in this paper is fully developed in the frame of deterministic application, which not only provides a preliminary prediction on the RCS fluctuation versus the spatiality information of the facets/wedges, but also has comparatively significant computational efficiency. The model may facilitate the

investigations and understandings on the mean levels of bistatic radar cross sections (RCS) returns from electrically large sea scene with ship-like targets. Several possible comments could be in order. First, tapered incident wave and short wave modification should be introduced to enhance the facet model, so that the phase distribution could be calculated more clearly, so as to take charge time evolving profiles. Second, non-Bragg mechanisms, as wedge scattering, white capping, and wave breaking, should be involved in the deterministic frame, for developing a more reliable facet model. Third, due to the consideration of computational efficiency, the approximate scheme employed to evaluate the multi-interaction between the incident wave and maritime scene is still comparatively simple, which limits the model also beyond the applications on very small grazing angles. Fourth, the nonlinear hydrodynamic of the sea waves and ship-sea interactions, bistatic SAR imagery applications, and time-evolving implementations, etc., will be under consideration in further research work.

ACKNOWLEDGMENT

REFERENCES

1. Fabbro, V., "Apparent radar cross section of a large target illuminated by a surface wave above the sea," *Progress In Electromagnetics Research*, Vol. 50, 41–60, 2005.

2. Luo, W., M. Zhang, Y.-W. Zhao, and H. Chen, "An efficient hybrid high-frequency solution for the composite scattering of the ship very large two-dimensional sea surface," *Progress In Electromagnetics Research M*, Vol. 8, 79–89, 2009.

3. Ji, W.-J. and C.-M. Tong, "Bistatic scattering from two-dimensional dielectric ocean rough surface with a PEC object partially embedded by using the G-SMCG method," *Progress In Electromagnetics Research*, Vol. 105, 119–139, 2010.

4. Zhang, M., Y. W. Zhao, H. Chen, and W.-Q. Jiang, "SAR imaging simulation for composite model of ship on dynamic ocean scene," *Progress In Electromagnetics Research*, Vol. 113, 395–412, 2011.

5. Bausssard, A., M. Rochdi, and A. Khenchaf, "PO/mec-based scattering model for complex objects on a sea surface," *Progress In Electromagnetics Research*, Vol. 111, 229–251, 2011.

6. Jin, Y. Q. and Z. X. Li, "Numerical simulation of radar surveillance for the ship target and oceanic clutters in two-dimensional model," *Radio Science*, Vol. 38, No. 3, 1045, 2003.

7. Yang, W., Z. Q. Zhao, C. H. Qi, W. Liu, and Z. P. Nie, "Iterative hybrid method for electromagnetic scattering from a 3-D object above a 2-D random dielectric rough surface," *Progress In Electromagnetics Research*, Vol. 117, 435–448, 2011.

8. Qi, C., Z. Zhao, W. Yang, Z.-P. Nie, and G. Chen, "Electromagnetic scattering and doppler analysis of three-dimensional breaking wave crests at low-grazing angles," *Progress In Electromagnetics Research*, Vol. 119, 239–252, 2011.

9. Ergul, O., "Parallel implementation of MLFMA for homogeneous objects with various material properties," *Progress In Electromagnetics Research*, Vol. 121, 505–520, 2011.

10. Colak, D., R. J. Burkholder, and E. H. Newman, "Multiple sweep method of moments analysis of electromagnetic scattering from 3D targets on ocean-like rough surfaces," *Microwave Opt. Technol. Lett.*, Vol. 49, No. 1, 241–247, 2007.

11. Jeng, S. K., S. W. Lee, M. H. Shen, H. S. Yuan, and L. Pong, "High frequency scattering from a ship at sea," *IEEE Trans. Antennas Propagat.*, Vol. 93, No. 5, 1436–1439, 1993.

12. Gao, P. C., Y. B. Tao, and H. Lin, "Fast RCS prediction using multiresolution shooting and bouncing ray method on the GPU," *Progress In Electromagnetics Research*, Vol. 107, 187–202, 2010.

13. Burkholder, R. J., P. Janpugdee, and D. Colak, "Development of computational tools for predicting the radar scattering from targets on a rough sea surface," Technical Report, Ohio State University Electro Science Laboratory, Columbus, Ohio, 2001.

14. Cui, K., X. J. Xu, and S. Y. Mao, "EM scattering of a special kind of cavities with applications to RCS calculation of targets over sea surface," *International Conference on Radar CIE*, 1–4, 2006.

15. Cui, K. and X. J. Xu, "EM scattering calculation for complex targets over sea surface," *IEEE Trans. Antennas Propagat.*, Vol. 3A, No. 6, 101–104, 2005.

16. Xu, X. J., Y. Wang, and Y. Qin, "SAR image modeling of ships over sea surface," *Proc. of SPIE*, Vol. 6363, 2006.

17. Dong, C. Z., C. Wang, X. Wei, and H.-C. Yin, "EM scattering from complex targets above a slightly rough surface," *PIERS*

Online, Vol. 3, No. 5, 685–688, 2007.

18. Wright, J. W., "A new model for sea clutter," *IEEE Trans. Antennas Propag.*, Vol. 16, 217–223, 1968.

19. Valenzuela, G. R., "Theories for the interaction of electromagnetic waves and oceanic waves: A review," *Bound. Layer Met.*, Vol. 13, 61–85, 1978.

20. Timchenko, A. I., "Model of electromagnetic wave scattering from sea surface with and without oil slicks", *Progress In Electromagnetics Research*, Vol. 37, 319–343, 2002.

21. Plant, W. J. and W. C. Keller, "Evidence of bragg scattering in microwave doppler spectra of sea return," *J. Geophys. Res.*, Vol. 95, 16299–16310, 1990.

22. Bass, F. G. and I. M. Fuks, *Wave Scattering from Statistically Rough Surfaces*, 418–442, Pergamon Press Oxford, New York, 1979.

23. Fung, A. K. and K. Lee, "A semi-empirical sea-spectrum model for scattering coefficient estimation," *IEEE J. Oceanic Engineering*, Vol. 7, No. 4, 166–176, 1982.

24. Zhao, Y.-W., M. Zhang, and H. Chen, "An efficient ocean sar raw signal simulation by employing fast fourier transform," *Journal of Electromagnetic Waves and Applications*, Vol. 24, No. 16, 2273–2284, 2010.

25. Park, J.-I. and K.-T. Kim, "A comparative study on ISAR imaging algorithms for radar target identification," *Progress In Electromagnetics Research*, Vol. 108, 155–175, 2010.

26. Hasselman, K., et al., "Theory of synthetic aperture radar ocean imaging: A MARSEN view," *J. Geophys. Res.*, Vol. 90, 4659–4686, 1985.

27. Andreas, A. B., A. Khenchaf, and A. Martin, "Bistatic radar imaging of the marine environment. Part I: Theoretical background," *IEEE Trans. Geosci. Remote Sens.*, Vol. 45, No. 11, 3372–3383, 2007.

28. Chen, H., M. Zhang, D. Nie, and H.-C. Yin, "Robust semi-deterministic facet model for fast estimation on EM scattering from ocean-like surface," *Progress In Electromagnetics Research B*, Vol. 18, 347–363, 2009.

29. Ward, K. D., C. J. Baker, and S. Watts, "Maritime surveillance radar. Part 1: Radar scattering from the ocean surface," *IEEE J. Oceanic Engineering*, Vol. 7, No. 4, 166–176, 1982.

30. Michaeli, A., "Equivalent edge currents for arbitrary aspects of observation," *IEEE Trans. Antennas Propagat.*, Vol. 32, 252–258,

1984.

31. Wu, Z. S. and M. Zhang, "Improved equivalent edge currents by modified edge representation and their application in EM scattering," *Acta Electronica Sinica* Vol. 26, No. 9, 1998.

32. Johnson, J. T., "A study of the four-path model for scattering from an object above a half space," *Microwave Opt. Technol. Lett.*, Vol. 30, No. 6, 130–134, 2001.

33. Shtager, E. A., "An estimation of sea surface influence on radar reflectivity of ships," *IEEE Trans. Antennas Propagat.*, Vol. 47, No. 10, 1623–1627, 1999.

34. Plant, W. J., "Studies of backscattered sea return with a CW, dual-frequency, X-band radar," *IEEE Trans. Antennas Propag.*, Vol. 25, 28–36, 1977.

35. Hasselmann, D. E., "Directional wave spectra observed during JONSWAP 1973," *J. Phys. Oceanogr.*, Vol. 10, No. 7, 1264–1280, 1980.

36. Luo, W., M. Zhang, C. Wang, and H.-C. Yin, "Investigation of low-grazing-angle microwave backscattering from three-dimensional breaking sea waves," *Progress In Electromagnetics Research*, Vol. 119, 279–298, 2011.

37. Okino, N., Y. Kakazu, and M. Morimoto, "Extended depth-buffer algorithms for hidden-surface visualization," *IEEE Computer Graphics and Applications*, Vol. 4, No. 5, 79–88, 1984.

38. Cox, C. and W. H. Munk, "Statistics of the sea surface derived from sun glitter," *J. Marine Res.*, Vol. 13, 198–227, 1954.

39. Ulaby, F. T., R. K. Moore, and A. K. Fung, *Microwave remote sensing*, Addison-Wesley Publishing Company, Canada, 1982.

40. Klein, L. A. and C. T. Swift, "An improved model for the dielectric constant of sea water at microwave frequencies," *IEEE Trans. Antennas Propagat.*, Vol. 25, No. 1, 1977.

41. Voronovich, A. G. and V. U. Zavorotni, "Theoretical model for scattering of radar signals in Ku- and C-bands from a rough sea surface with breaking waves," *Waves in Random and Complex Media*, Vol. 11, No. 3, 247–269, 2001.

42. Awada, A., M. Y. Ayari, A. Khenchaf, and A. Coatanhay, "Bistatic scattering from an anisotropic sea surface: Numerical comparison between the first-order SSA and the TSM models," *Waves in Random and Complex Media*, Vol. 16, No. 3, 383–394, 2006.

43. Kozlov, A. I., L. P. Ligthart, and A. I. Logvin, *Mathematical and Physical Modelling of Microwave Scattering and Polarimetric*

Remote Sensing — Monitoring the Earth's Environment Using Polarimetric Radar: Formulation and Potential Applications, 43–65, Kluwer Academic Publishers, New York, 2001.

44. Zhang, M., H. Chen, and H.-C. Yin, "Facet-based investigation on EM scattering from electrically large sea surface with two-scale profiles: Theoretical model," *IEEE Trans. Geosci. Remote Sens.*, Vol. 49, No. 7, 2011.

45. Plant, W. J., "Microwave sea return at moderate to high incidence angles," *Waves in Random and Complex Media*, Vol. 13, No. 4, 339–354, 2003.